4

Chemical Force Microscopy: Force Spectroscopy and Imaging of Complex Interactions in Molecular Assemblies

Dmitri V. Vezenov, Aleksandr Noy, and Charles M. Lieber

1 Introduction

Many macroscopic processes and events in condensed phases are driven by intermolecular interactions that extend beyond the basic pair-wise adhesive interactions of functional groups that were the focus of the previous chapter. The spectrum of these interactions ranges from the long-range forces that by necessity involve large ensembles of functional groups, to friction and wear processes that involve constant breaking and reforming of noncovalent bonds at different length and time scales. Often these interactions are accompanied by substantial energy dissipation, and thus rigorous quantitative treatment of these events becomes a considerable challenge.

Despite such difficulties, Chemical Force Microscopy (CFM) provides an excellent opportunity to probe these events with an unprecedented degree of chemical specificity. We first describe the use of CFM for probing ionization processes at surfaces. The long-range nature of Coulombic interactions and double-layer formation in aqueous solutions of electrolytes leads to the involvement of a large number of species both in solution and on the surfaces, and the interplay between these species gives rise to complex processes such as charge regulation. We show how rational control over the chemical functionality of the atomic force microscope (AFM) probe allows local probing of these processes and provides information about the ionization state of the surface functional groups.

Monitoring friction at the local scale provides an excellent opportunity to study the role of specific interactions in this complex dissipative process. Extreme curvature of the AFM tip provides a convenient system for studying single asperity constants, and CFM measurements provide an ideal vehicle for probing the fundamentals of the friction forces. On a molecular level, friction process involves repeated breaking of noncovalent bonds; therefore, we need to control the chemistry at the sheared interface to probe the link between adhesion and friction forces in these idealized model systems.

An important extension of the friction force studies is the use of chemically-functionalized AFM tips for rational imaging of surface functional groups. We describe how the observations of chemical sensitivity in friction forces translate into the chemically-sensitive imaging of surface patterns of functional groups. Besides representing an immensely important subset of the AFM-based imaging techniques, tapping (intermittent-contact) mode imaging provides an

opportunity for direct probing of the energy dissipation in the tip-sample junction; and we show that chemical modification of the AFM probes provides us with an opportunity to tune these interactions. Overall, chemical modification of the AFM probes gives a versatile and powerful method for probing the dynamic of complex intermolecular interactions in condensed phases.

2 Probing Adhesion Forces in Molecular Assemblies Bearing Charges

2.1 Chemical Force Titrations: Operating Principle

The acid-base chemistry of ionizable sites immobilized at interfaces is central to understanding a number of complex dispersed systems, such as micelles, nanoparticles, polymers, polyelectrolytes, and biological macromolecules, thus making water an important medium for CFM experiments. The charged state of the surfaces is of fundamental interest in colloidal stability, particle adhesion to surfaces, and adsorption of macromolecules.[1, 2] An important consideration for these systems is that the dissociation constants of the surface groups can differ from those of their monomer analogs in solution. Several factors can cause these differences: (i) a low dielectric permittivity of an adjacent hydrocarbon region; (ii) fewer degrees of freedom for the immobilized species; (iii) an excess electrostatic free energy of the supporting surface; and (iv) changes in the solution dielectric constant in the vicinity of charged surfaces.[3] While a theoretical description must make estimates of these considerations, CFM includes these factors by design.

The surface free energy depends on the state and the degree of ionization of the functional groups, which can be monitored by measuring a contact angle of a buffered droplet versus pH of the drop solution. A large change in the contact angle occurs at a pH equal to the pKa of the surface groups, when half of the maximum number of ionizable groups have dissociated.[4] Chemically-modified AFM tips provide an alternative way to probe such changes in solid-liquid surface free energies with pH. The surface charge induced by the dissociation of acidic/basic groups can be detected by monitoring the adhesive force with an AFM probe sensitive to electrochemical interactions, and variations in the sign and magnitude of the interactions will indicate changes in the surface charge: a transition from adhesion to repulsion will occur at a pH≈pK of the functional group on the surface. This AFM-based approach to determining local pKs has been termed "chemical force titration" (CFT) by Lieber and co-workers.[5]

CFT probes pH dependence of adhesion forces between basic or acidic functional groups, or more generally, dependence of adhesion forces between ionizable groups as a function of the concentration of counterions. Several aspects of ionization of surface groups have been investigated with CFM: (i) large pK_a shifts of amine-terminated SAMs; (ii) observation of inverted CFT curves for aromatic amines; (iii) effect of ionic strength (IS) on the shape of the CFT curves and peak positions; and (iv) ion adsorption by neutral groups.

Adhesion force values measured at different solution pH for tips and samples functionalized with 3-aminopropyltriethoxysilane (APTES) SAMs terminating with amine groups show a sharp drop to zero (indicating a repulsive interaction) below a pH of 4 (Figure 1A). This decrease and elimination of an attractive force between the tip and sample at low pH is consistent with the protonation of the amine groups on these two surfaces. Contact angle values measured using buffered solution droplets on this surface (Figure 1B) also show a sharp transition (an increase in wetability) as the droplet pH is reduced below 4.5. Hence local force microscopy measurements using a modified probe tip and macroscopic wetting studies provide very similar values for the pK of the surface amine group in the APTES-derived SAMs.

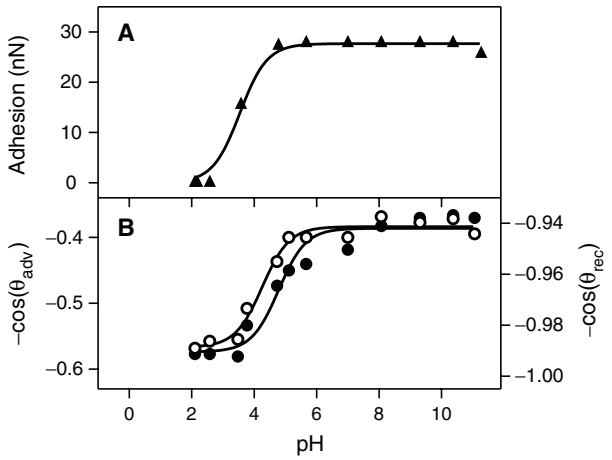

Figure 1. (A) Adhesion force between sample and tip functionalized with amino groups versus pH (B) Negative cosines of the advancing (open circles) and receding (filled circles) contact angles of phosphate buffer drops on a Si sample modified with APTES as a function of pH.

The apparent pKa obtained from force microscopy (pK = 3.9) and contact angle wetting (pK = 4.3) for the surface amine group is 6–7 pK units lower than bulk solution values.[6] Similarly, large pK_a shifts and strong adhesion at high pH were found for thiolate long-chain (-$(CH_2)_{11}$-) SAM pairs bearing amine functionality.[7] Large shifts in dissociation constants observed in CA titrations for mixed acid-methyl monolayers were attributed to unfavorable solvation of the carboxylate anion at the monolayer interface.[8] Large pK shifts relative to solution were also observed in studies of amino groups grafted onto the surface of a hydrophobic polymer.[9] In addition, simulations of the titration of surface amine groups showed large negative shifts in pK when the amine was poorly solvated.[10] Since the interfacial tension in alkylamine-water system is negligibly small (< 0.1 mJ/m^2),[11] the high contact angles and large adhesion forces at pH > 4 indicate that the APTES-derived monolayers are relatively hydrophobic. The hydrophobic nature of the SAM likely arises from a partially disordered structure that exposes methylene groups at the surface. Hence one can attribute the large observed pK shift to a hydrophobic environment surrounding the amine groups. A vapor-phase deposition procedure[12] improves the quality of the APTES modification of SiO_2/Si substrates, and this silanization method produces reproducible monolayers with a higher $pK_{1/2}$ (7.4) and a factor of three lower adhesion forces. On the other hand, increasing the chain length from 2 to 11 methylene units of analogous amine-terminated thiol SAM did not result in significant $pK_{1/2}$ changes. Notably, the measured adhesion force, F_a, was larger for a short-chain pair than for a long-chain pair as expected from the degree of ordering in these SAMs.[13]

The ability to detect such pK changes locally by AFM should be of significant utility to studies of biological and polymer systems. Several studies have already demonstrated the potential of the technique: He et al. demonstrated the local character of pK_a measurements with CFT by observing $pK_{1/2}$ of 5.6 for COOH SAM on micropatterned substrates (1–2 µm regions terminating in COOH or CH_3), for which contact angle titration showed a transition at $pK_{1/2}$ = 11.0,[14] and the Vancso group reported a remarkable spatial resolution of ca. 50 nm for CFT of plasma treated polymer substrates.[15, 16]

CFT of basic functional groups, in which a nitrogen atom is involved with aromatic functionality (either being a part of the aromatic ring, as in 4-mercaptopyridine HS-Py, or through conjugation, as in 4-aminothiophenol HS-Ph-NH_2), produced high adhesion force

at low pH and low/repulsive forces at high pH—contrary to expectations based on their charged state.[17, 18] To explain this phenomenon, *ab initio* calculations of surface charges were carried out for APTES, HS-Ph-NH_2, and HS-Py molecules.[19] Calculated surface charges (in units of electron charge) for these groups were, respectively, 0.606, 0.607, and 0.035 in the protonated state, and −0.09, −0.298, and −0.909 in the neutral state. A highly polarized state of Py groups together with efficient charge dispersion in Py-H^+ is consistent with repulsion between neutral Py groups and attraction between charged Py-H^+ groups observed in CFTs. A significant surface charge of Ph-NH_2 groups is responsible for low adhesion at high pH. Protonated Ph-NH_3^+ groups, however, carry the same charge as primary amine APTES. Since some fraction of neutral groups carrying comparable and opposite surface charge (−0.3 vs 0.6) is available at low pH, the observed adhesion reflects the interaction between surfaces with reduced overall charge and having a distribution of positive (due to Ph-NH_3^+) and negative (due to Ph-NH_2) local charge.

2.2 Chemical Force Titrations on Hydrophilic Surfaces

Contact angle goniometry is limited to sufficiently hydrophobic surfaces that do not show complete wetting in both non-ionized and ionized states. In the case of high free energy surfaces, such as COOH terminated SAMs, it is necessary to dilute the hydrophilic groups with a hydrophobic surface component and either pretreat the surface[8] or use another liquid (vs. vapor phase)[20] to perform a contact angle experiment. As CFT results on the APTES system demonstrate, the incorporation of a hydrophobic component must be used with considerable caution, since it can produce very large pK shifts. Such shifts in the pK_a of surface COOH relative to bulk solution have been observed in cases of mixed COOH and $CH_3$3 SAMs.[8, 20] Hence it has not been possible to determine the pK of a homogeneous COOH-terminated surface by the contact angle approach.

In contrast, force titrations provide a direct measure of the solid-liquid interfacial free energy and completely bypass the limitations discussed in the previous paragraph. A prominent feature in the force titration curve obtained for COOH-terminated sample and tip (Figure 2A) is the sharp transition from positive adhesion forces at low pH to zero (indicating repulsion) at high pH. The observed repulsion at pH>6 can be attributed to interaction between electrical double layers formed in the presence of charged carboxylate groups, while the adhesive interaction at low pH values originates from hydrogen bonding between uncharged carboxyl groups. The force versus separation curves become fully reversible and practically identical at all pH values higher than 7. This indicates that the surface charge density is saturated under these conditions. Based on these CFT data, the pK_a of the surface-confined carboxylic acid is 5.5 ± 0.5. This value lies within 0.75 pK units of the pK_a for COOH functionality in aqueous solution.[6] The similarity of surface-confined and solution pK_as strongly indicates that solvation effects do not play a significant role in determining the ionization behavior of pure COOH-terminated SAMs.

Control experiments with both hydrophilic and hydrophobic groups that do not dissociate in aqueous solutions do not display pH-dependent transitions. CFM titration curves for tip/sample SAMs terminating in OH/OH and CH_3/CH_3 functionalities show an approximately constant, finite adhesive interaction throughout the whole pH range studied (Figure 2B). To probe pKs on unknown surfaces, we need to use tips functionalized with SAMs that (i) do not exhibit a pH-dependent change in ionization and (ii) are hydrophilic. The hydroxyl-terminated SAM meets these requirements, and has been used to determine the pK_a of carboxyl-terminated SAM as shown in Figure 2C. Remarkably, the dissociation constant obtained from that titration curve is the same as that determined from the data in Figure 2A using COOH-terminated SAMs on both sample and tip.

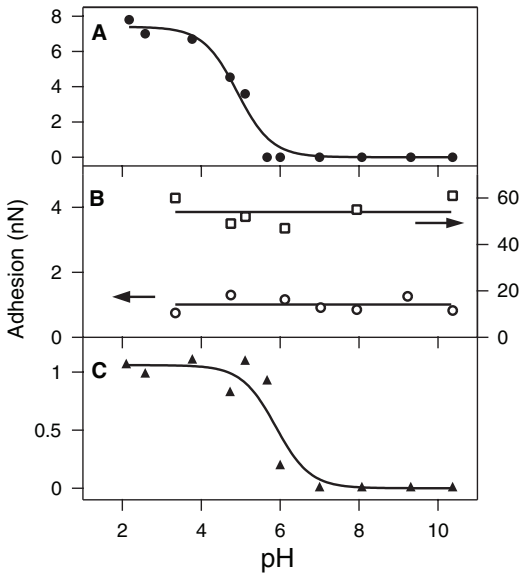

Figure 2. CFT curves recorded in buffered solutions (ionic strength of 0.01 M) for (A) COOH-COOH; (B) CH_3-CH_3 (squares) and OH-OH (circles); and (C) COOH-OH contacts 5.

Wong et al. achieved the ultimate resolution of CFT by applying it to identify the functional groups at the terminus of chemically modified carbon nanotubes (CNTs).[21, 22] Shortening the CNT by an electrical arc discharged in the presence of oxygen resulted in termination of the CNT with carboxylic acid groups. CFT of such CNT showed adhesion curves (Figure 3) similar to those of analogous SAMs systems (Figure 2A). Subsequent chemical modification of the nanotube ends to amine functionality resulted in titration curves characteristic of basic functional groups. Alternatively, a COOH functional group at the CNT end could be converted chemically into neutral benzyl moiety, for which CFTs no longer displayed the transitions as expected when dissociation of surface groups cannot occur.

2.3 Peaks in CFT Curves Due to Hydrogen Bonding and Ion Bridges

CFT at low ionic strength ($<10^{-4}$ M) resulted in another type of unusual behavior: instead of a sigmoidal transition from the high adhesion between neutral groups to low adhesion (or repulsion) between charged groups, Smith et al. observed a peak in adhesion force at intermediate pH for COOH,[23–25] $PO(OH)_2$,[24–26] and NH_2[13] groups. Their interpretation of 10- to 20-fold increase of adhesion between hydrophilic groups centers on a hypothesis of formation of "strong hydrogen bonds" between neutral and charged groups representing a conjugated acid/base pair, e.g., carboxyl and carboxylate. For a given fraction β of dissociated groups, the total adhesion force is comprised of two contributions from a total of N groups: (i) "weak" hydrogen bonds between neutral groups (e.g., COOH/COOH) with a single force value of f_{hb} and (ii)"strong" ionic hydrogen bonds (e.g., COOH/COO^-) that are a factor of m stronger:

$$F_a = N f_{hb} \left[2\left(1-\beta\right)\beta\, m + \left(1-\beta\right)\left(1-\beta\right) m \right] \tag{1}$$

Smith and co-workers were able to reproduce the shape of the CFT peak with the equation above for $HS(CH_2)_{15}COOH$ SAMs resulting in a fitted value $m \approx 16$ (Figure 4), although for shorter $HS(CH_2)_{10}COOH$ SAM, the observed peak was wider than predicted.[23]

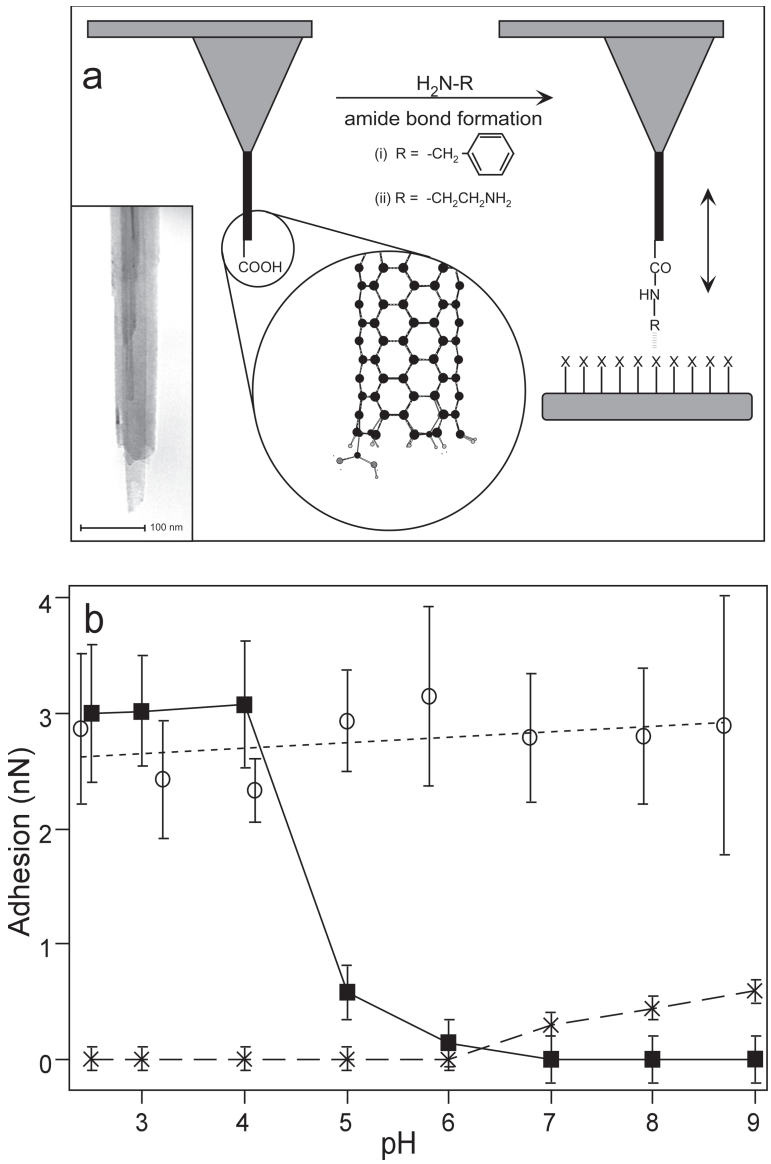

Figure 3. (A) Diagram illustrating the modification of a nanotube tip by coupling an amine (RNH_2) to a pendant carboxyl group, and the application of this probe to sense specific interactions with functional groups (X) of a substrate. The circular inset is a molecular model of a single nanotube wall with one carboxyl group at the tip end. Inset, TEM image showing the open end of a shortened nanotube tip. (B) Adhesion force as a function of pH between the nanotube tips and a hydroxy-terminated SAM (11-thioundecanol on gold-coated mica): filled squares, carboxyl (unmodified); open circles, phenyl (modified with benzylamine); and crosses, amine (modified with ethylenediamine). Each data point corresponds to the mean of 50–100 adhesion measurements, and the error bars represent one standard deviation. From Ref. 21.

Since the relevant forces reflect the energy balance for interactions between groups on the tip and sample as well as these same surface groups and the solvent, one needs to take these arguments as reflecting the difference in the strength of the respective hydrogen bonds between carboxylate anion and carboxylic acid group on the one hand, and carboxylate anion and water on the other hand. Differences in hydrogen bond strength could partly reflect differences in the dielectric constant of the environment surrounding charged groups

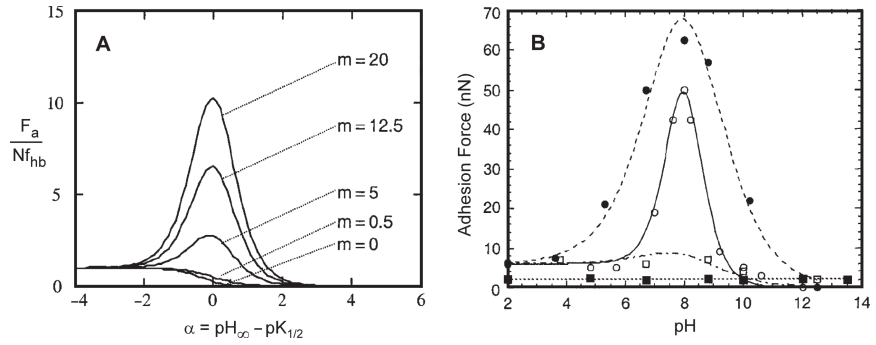

Figure 4. (A) The CFT curves are modeled as a linear combination of two types of hydrogen bonds—strong ionic and weak neutral bonds—and plotted for different values of m (the ratio of the strength of these two bonds). pH_∞ is the pH of the bulk solution, and $pK_{1/2}$ is defined as the pH at which half of the surface groups are ionized. The peak in CFT observed for the low electrolyte concentration is reproduced with values of m = 15–20, whereas the sigmoidal step at high ionic strength is reproduced by m~0, i.e., no strong hydrogen bonds formed (e.g., because of the interaction of ions in the buffer with the ionized acid groups in the SAMs). (B) Effect of SAM packing on CFT curves in a buffer of very low electrolyte concentration (10^{-7} M) for tips and substrates modified with $HS(CH_2)_{15}COOH$ (16:16, open circles), $HS(CH_2)_{10}COOH$ (11:11, solid circles), $HS(CH_2)_{10}COOH$ and $HS(CH_2)_3COOH$ (11:3, open squares), and $HS(CH_2)_3COOH$ (3:3, solid squares). The 16:16 peak is accurately fitted by Equation 1, yielding a value of m = 16), while the rest of the curves (11:11, 11:3, and 3:3 data) are only guides to the eye.

when exposed to water, or when sandwiched between organic SAMs. Similarly shaped CFT curves were observed for $(HS(CH_2)_{11}O)_2PO(OH)$ modified tips and surfaces.[27] One caveat of this model is that while the peak in adhesion force is predicted for $\beta = ½$, the $pK_{1/2}$ values should be more appropriately treated as pH values where adhesion force takes ½ its maximum value, rather than pH for the degree of dissociation of 0.5 for surface groups. An analysis of the noncontact regime of CFT with force feedback showed that the surface potential of COOH groups at pH = 7 reflects the maximum β value of about 15%,[28] while surface charge calculation gives the pK_a of 7.7. Simultaneous analysis of contact (adhesion) and noncontact (double layer) forces appears to be the most consistent way for determining the pK_a of surface functional groups.

CFT of neutral surfaces that can form complexes with ions from solution can result in a sandwich-type interfacial bond: adhesion between methylsulfanyl groups on the tip and sample in a solution of $AgNO_3$ (IS = 0.1 M, KNO_3) showed a peak at $p[Ag^+] = 2$, while adhesion between similarly prepared hexyl monolayers was insensitive to variations in Ag^+ concentration.[29] A model of binding was proposed that involved formation of 1:2 interfacial complexes, $R(CH_3)S\text{-}Ag^+\text{-}S(CH_3)R$, that promoted strong interfacial bonds at a low concentration of silver ions. At a high concentration ($>10^{-2}$ M) of Ag^+, the surface coverage increased (approached saturation): competitive repulsion from $R(CH_3)S\text{-}Ag^+/Ag^+\text{-}S(CH_3)R$ interactions resulted in a sharp drop in adhesion. Interestingly, detailed analysis of a noncontact regime in CFTs on nominally neutral surfaces—hydrophobic, methyl-terminated, and hydrophilic, ethylene oxide-terminated—revealed that both interfaces can undergo complex charging as a function of solution pH via adsorption of hydronium and hydroxyl ions.[30]

2.4 Modeling of Adhesion Forces in the Presence Charge

The JKR theory of contact mechanics (see chapter 3) can serve as a reasonable basis for understanding adhesion data in an aqueous medium. To interpret pH dependent adhesion data in electrolyte solutions it is also important to consider long-range electrostatic forces between the tip and sample surface. Since the JKR theory is based on energy balance, it is reasonable

to expect no adhesion (i.e., Hertzian behavior) when the free energy of a double layer per unit area w_{DL} balances the interfacial surface tension γ_{SL}. Quantitatively, the pull-off force, $P_{pull\text{-}off}$, can be related to these two terms as follows:

$$P_{pull-off} - P_{DL} = -\frac{3}{2}\pi R(W_{SLS} - 2w_{DL}),\ or\ P_{pull-off} = -\frac{3}{2}\pi R W_{SLS} + \frac{5}{2}P_{DL} \quad (2)$$

where $P_{DL} \approx 2\pi R w_{DL}$ is an additional load that has to be applied to a spherically shaped tip due to the presence of a double layer. Thus, repulsion between like-charged surfaces ($P_{DL}>0$) will decrease the magnitude of the pull-off force compared to that given by the JKR theory. There is a threshold value of the repulsive electrical double layer force $P_{DL} = P_{pull\text{-}off}$, beyond which the deformation of a spherical tip should be fully reversible with a contact radius going monotonically to zero (no pull-off force) as the load is reduced. This condition is equivalent to $\gamma_{SL} \approx w_{DL}$; that is, the attractive surface free energy component is canceled by the repulsive double layer term. The corresponding surface potential

$$\Psi = \sqrt{\frac{\lambda}{\varepsilon\varepsilon_0}\gamma_{SL}} \quad (3)$$

is independent of the tip radius for $\lambda << R$ (λ is the Debye length, ε is the dielectric constant, and ε_0 is the permittivity of vacuum). Therefore, the change from adhesive to repulsive behavior is characteristic of the ionization state of the interacting surfaces and can be used to estimate the surface potential.

This model allows us to calculate the surface free energies and surface potentials of hydrophilic SAMs. The values of γ_{SL} determined from adhesion data for OH and COOH (fully protonated) terminated surfaces were 8 mJ/m^2 and 16 mJ/m^2, respectively, and are in good agreement with the measurements of interfacial tension for the two-phase systems consisting of water and melts of either long-chained alcohols (7-8 mJ/m^2)[31] or carboxylic acids (10-11 mJ/m^2).[32] The surface potential of the carboxylate SAM at pH>6 and ionic strength of 0.01 M, 65 mV, calculated from Equation 3, is substantiated by analysis of F-D curves discussed in the next section.

2.5 Probing Double Layer Forces

The electrochemical origin of the pH-dependent repulsive forces can be verified by changing the Debye screening length λ; (i.e., by changing the solution ionic strength). The repulsive interaction becomes progressively longer-ranged (Figure 5, left panel) as the solution ionic strength decreases. A detailed analysis of the electrical double layer forces must take into account the surface charge-potential regulation imposed by the potential dependent binding of counterions (H^+ and Na^+ in the case of COOH SAMs) at the interface; for example, by using a model with a linearized condition for charge-potential regulation.[33] For carboxylate surfaces, this model fitted the experimental data very well down to separations of 1 nm. The condition of constant charge (vs. constant potential) was approached in these experiments independently of the ionic strength. The values of the Debye screening length extracted from experimental F-D curves agree well with the values calculated from the solution ionic strengths. Significantly, the surface potential calculated using this analysis of the carboxyl terminated surface at pH = 7.2 and 0.01 M ionic strength, 60 mV, is close to the value estimated from adhesion measurements.

Thus, it is possible to determine double layer parameters of systems being imaged by simultaneously recording F-D curves, using a tip bearing a functional group with a predetermined ionization behavior. Force-distance curves obtained with magnetic force feedback removed the jump-in instability and allowed recording of the full force profile for both neutral OH and charged COOH groups.[28] The F-D curves in the case of OH SAMs showed only

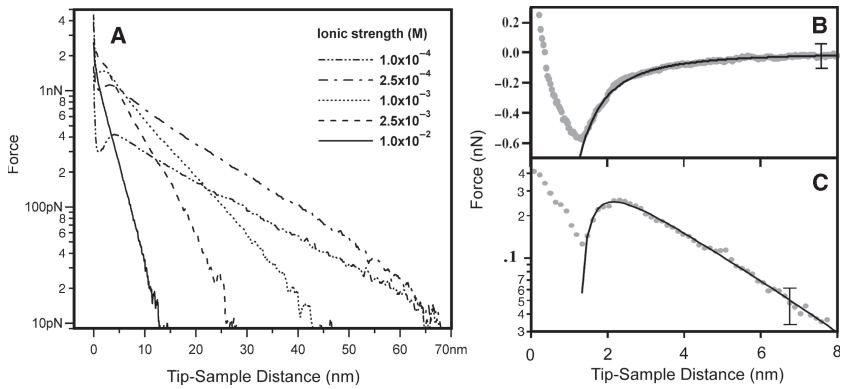

Figure 5. (A) Repulsive double layer forces versus tip-sample separation recorded on approach between COOH modified tips and samples at different ionic strengths of the pH 7.2 buffer. (B, C) Force profiles obtained using magnetic force feedback for (B) OH-terminated SAMs in deionized water and (C) COOH-terminated SAMs in 0.01 M, pH 7 phosphate buffer. Circles: Experimental data; Lines: model fits. The error bars are representative of the respective data sets 5.

attraction, whereas in the case of COOH SAMs double layer repulsion dominated van der Waals attraction at long (> 2 nm) distances.

3 Chemical Effects in Friction Experiments

CFM experiments on multiple organic monolayer systems demonstrated that friction and adhesion forces correlate at the nanometer scale. The friction force between functional groups on a sample surface and the tip is usually determined by recording the lateral deflection of the cantilever as the sample is scanned in a forwards/backwards cycle along the direction perpendicular to the cantilever axis to produce a friction loop.[34] The externally applied load is controlled independently through the cantilever normal deflection. The numerical values of the normal and lateral forces are determined using the cantilever spring constants, and friction coefficients are obtained from the slopes of the corresponding friction versus load (F-L) curves.

CFM uses chemically modified tips bearing well-defined functional groups to assess unambiguously chemical contributions to friction. As mentioned in the section on the mechanics of tip-substrate contact in the preceding chapter, one has to be careful in selecting conditions for quantitative analysis of chemical effects on frictions force. Ideally, such characterization comes from comparison of values of the shear stress for each functional group pair. These values are rarely available, because they require accurate knowledge of mechanical and geometrical parameters of the system (cantilever constants, tip radii, effective elastic constants of monolayer-substrate contact). Quantitative *comparison* of different functional groups in CFM is frequently achieved by ensuring that the systems are structurally similar by using (i) the same monolayer system (i.e., thiol SAMs on polycrystalline gold) and (ii) CFM tips of similar characteristics (or the same tip with different surfaces/media).

In ambient conditions, it is difficult to distinguish clearly true chemical contributions to friction from other factors primarily due to the large magnitude of capillary adhesion. This effect can be eliminated by performing measurements either in liquids or ultrahigh vacuum. Friction forces between tips and samples modified with different functional groups have been measured in ethanol,[35] water,[5] and dry argon[36] as a function of an applied load. In all of these measurements, the friction forces were found to increase linearly with the applied load. For a

fixed external load the absolute friction force decreased as COOH/COOH > CH_3/CH_3 > COOH/CH_3[35, 36], as shown in Figure 6. The trend in the magnitude of the friction forces and friction coefficients is the same as that observed for the adhesion forces: COOH/COOH-terminated tips and samples yield large friction and adhesion forces, while the COOH/CH_3 combination displayed the lowest friction and adhesion. Thus, there is a direct correlation between the friction and adhesion forces measured between well-defined SAM surfaces.

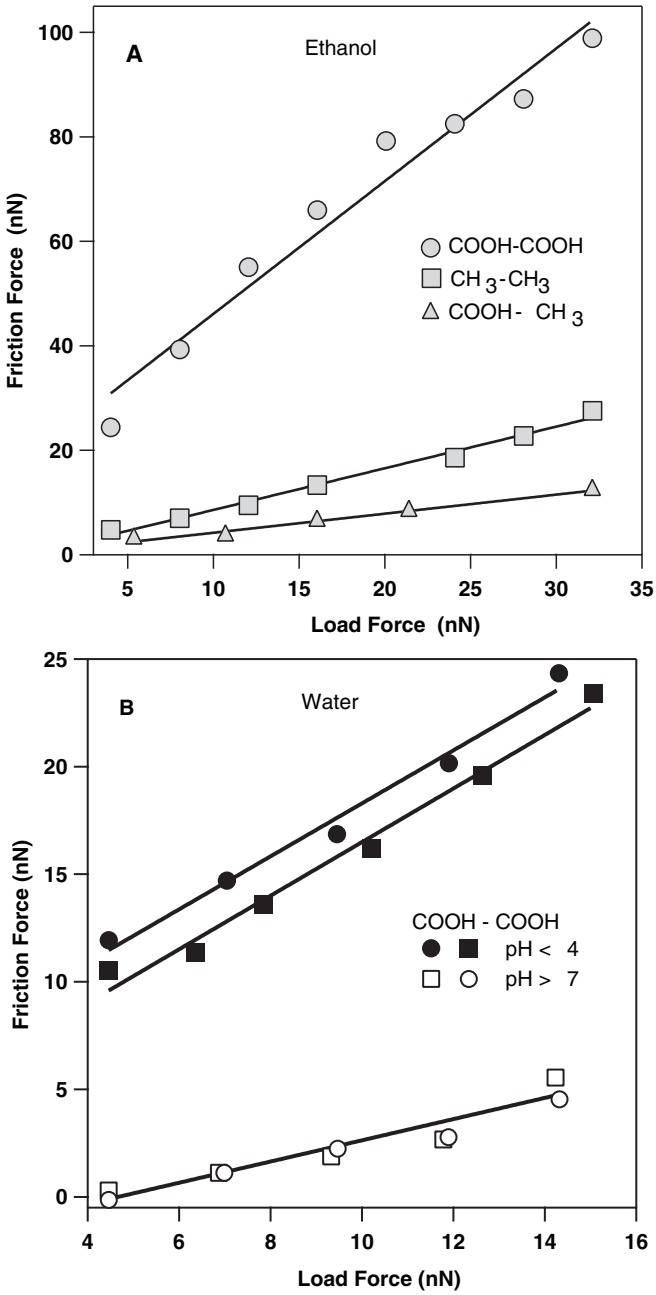

Figure 6. (A) Summary of the friction force versus applied load data recorded for functionalized samples and tips terminating in COOH/COOH (○), CH_3/CH_3 (□) and COOH/CH_3 (△) in EtOH. (B) Friction force versus applied load curves for COOH-COOH functionalized samples and tips recorded at pH below and above pK_a of surface carboxyl group.

The change in the ionization state of functional groups can also be detected by recording frictional forces at different pH. F-L curves for COOH-terminated tips and samples are linear, but fall into two distinct categories: larger friction forces and friction coefficients are found in solutions at pH < 6 compared to pH > 6 (Figure 6). This crossover in behavior occurs at the same region of pH where the normal forces exhibit a transition from attraction to repulsion. There is also a finite load (~4 nN, for the data in Figure 6) necessary to achieve nonzero friction at high pH. This additional load is required to overcome the double layer repulsion (between charged surfaces) and bring the tip into physical contact with the sample surface.

The frictional behavior of tips and samples functionalized with ionizable and non-ionizable SAMs can be summarized in plots of the friction coefficient versus pH. The friction coefficients determined for OH- and CH_3-terminated SAMs are independent of pH, as expected for neutral, non-ionizable functional groups. In contrast, the friction coefficients determined for cases in which one or both SAM surfaces terminate in carboxyl groups show significant decreases at pH above the pK_a of the surface COOH group. The friction coefficients therefore exhibit similar pH dependencies to those observed in adhesion measurements shown in Figure 2. These results suggest that the drop in friction coefficient with changes in pH is also associated with the ionization of surface groups.

The magnitudes of the friction force and friction coefficient for hydroxyl-terminated surfaces were the lowest among hydrophilic group pairs (COOH-COOH, COOH-OH, OH-OH) in aqueous solution. Analysis of F-L curves for methyl terminated tip/sample combinations also yields low friction coefficients; however, for comparable tip radii the magnitude of the friction force at low external loads is almost an order of magnitude greater than for either carboxyl or hydroxyl functionalized surfaces. The large magnitude of the friction force between methyl surfaces in aqueous media originates from the large contact area between hydrophobic surfaces.

Other monolayer properties can affect adhesive and frictional behavior of organic layers. For example, AFM studies of phase-segregated Langmuir-Blodgett films have indicated that elasticity and crystallinity correlate with observed friction[37] and adhesion.[38] Chain-length dependence was observed for friction on silane SAMs on mica[39] and LB films of saturated carboxylic acids.[40] This chain-length dependence may in part reflect structural differences in the different monolayers versus intrinsic viscoelastic effects.[39] Therefore, some additional information on mechanical properties of these SAMs may be required to ascribe observed differences in adhesion and friction to chemical effects in structurally well-defined systems.

4 Chemical Imaging Contrast in CFM Experiments

Scanning force microscopy (SFM) has transformed the fields of nanoscience and surface science by providing visualization in real space of structures and features of molecular and nanometer sizes. Initially, the images available with SFM could be interpreted as ultra-high resolution profilometry, which provides very limited information about sample properties and composition. Thus one clear goal for the development of the AFM imaging capabilities has always been achieving some degree of chemical sensitivity. Such sensitivity to the surface composition combined with unparalleled resolution can make force microscopy a versatile surface analysis tool. The contrast in AFM images originates from the interactions between the probe tip and the surface. In general, these interactions depend on the surface chemistry, morphology, mechanical properties, and on the nature of the surrounding medium. Thus, if we want chemical contrast to be the dominant contribution to the AFM image, it is necessary to identify and enhance forces that are chemically specific and eliminate interactions that are not correlated with the chemical identity of the functional groups at the interface. If the origin of the chemical contrast is understood, one can envision fine-tuning the probe-surface interac-

tions, or even the operating conditions of the instrument, as a way of enhancing the imaging sensitivity and specificity.

The CFM approach, which focuses on the chemical modification of the AFM tips as a way of probing and enhancing specific interactions, represents a logical first step for such an approach. We note that CFM, like any force spectroscopy approach, fundamentally relies on intermolecular, typically non-covalent, interactions to discriminate between different functionalities. Therefore, it may not achieve the identification power of other surface analysis techniques, such as secondary ion mass spectroscopy, or infrared spectroscopy. The spatial resolution of CFM, on the other hand, is orders of magnitude better than the lateral resolution of these other techniques. This high resolution, taken together with the applicability of AFM to a wide range of samples, offsets these inherent drawbacks. We now describe several CFM approaches that researchers have used to obtain maps of the surface that could be rationally interpreted on the basis of the tip-sample interactions.

4.1 Lateral Force Imaging

The results presented in the previous sections show that chemical modification of probe tips is often sufficient to influence normal and lateral forces in a rational way. Specifically, the observed differences in friction forces could readily produce lateral force images of heterogeneous surfaces with predictable contrast.[5, 35, 36, 41] Patterned SAMs of alkane thiols on Au surfaces present a convenient model system for such studies, because they represent an ideal model surface that exhibits chemical contrast. Patterned SAMs have homogeneous mechanical properties throughout the sample, are readily prepared, and can incorporate a variety of different terminal functionalities. In addition, patterned surfaces can be made relatively flat, thus eliminating unwanted topographic contributions to lateral force images. Indeed, a topographical image (Figure 7A) of a photochemically patterned SAM[42] that has 10 μm- × 10 μm-square regions terminated with -COOH groups and surrounded with CH_3-terminated groups is almost completely flat (certainly, a topographical image fails to distinguish the pattern!). Yet the friction maps of these samples taken with different tip functionality readily show contrast that reveals chemical information about the surfaces (Figures 7B, 7C). Friction maps recorded with COOH tips display high friction on the area of the sample that terminates in COOH groups, and low friction on the CH_3 terminated regions. Images recorded with CH_3 tips exhibit a reversal in the friction contrast: low friction is found in the area of the sample that contains the COOH-terminated SAM, and higher friction is observed in the surrounding CH_3 regions.

As expected, this reversal in friction contrast occurs only with changes in the probe tip functionality and is consistent with the friction forces obtained on the homogenous SAM surfaces. As typical for the friction-based measurements, the image resolution is not that of a single functional group but rather an ensemble of groups defined by the tip contact area. The apparent resolution in the images shown in Figure 7 is limited by the resolution of the photopatterning method used in preparing the sample (~200 nm). Employing a microcontact printing technique for pattern generation does improve the resolution by a factor of 4.[43] Researchers have achieved much higher resolution (on the order of 10–20 nm) using a monolayer-bilayer $COOH/CH_3$ system with functionalized tips in dry Ar atmosphere.[36]

The imaging contrast could be enhanced further by changing the solvent characteristics, such as composition[44] or pH[5]. We have demonstrated the validity of this approach by mapping changes in functional group ionization states with varying solution pH values. Images of COOH/OH patterned surfaces obtained with a COOH-terminated tip in different pH solutions show that the friction contrast between COOH/OH regions can be reversibly inverted, with the change in contrast always occurring near the pK_a of the surface carboxyl (Figures 7E, 7F). The reversals in friction contrast presented in these examples occur only with changes in the probe tip functionality in organic media or a change in the probe tip ionization state in aqueous

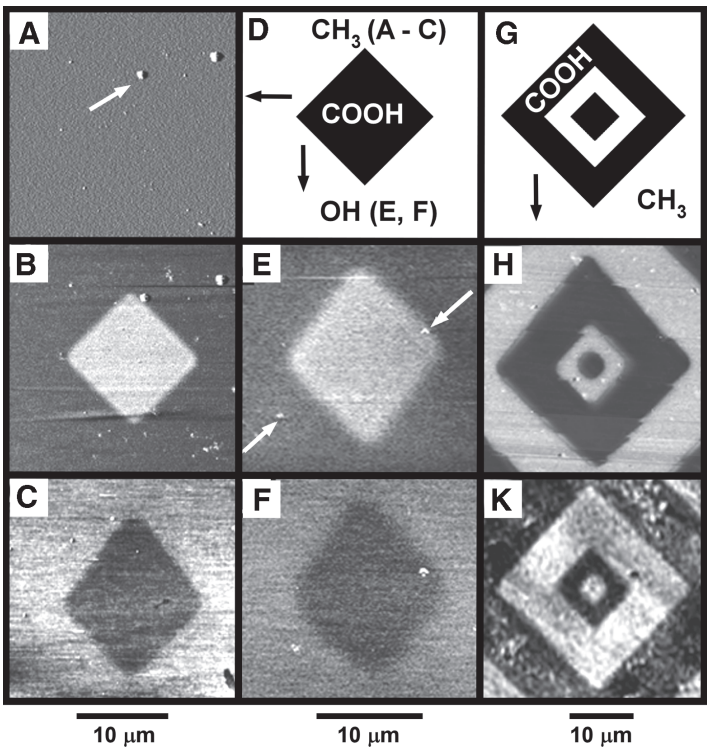

Figure 7. CFM images (dark gray represents areas of low friction, light gray represents areas of high friction) of photochemically generated patterns: $COOH/CH_3$ groups, image taken with COOH (A – topography, B – friction) or CH_3 (C) tips in ethanol; COOH/OH groups, image taken with COOH tips in 0.01 M phosphate buffer at low (E) and high (F) pH; $COOH/CH_3$ groups, image taken with CH_3 tips in water (H) or ambient air (K). Arrangement of the chemical functionality on the surfaces is outlined in (D) and (G). The same area of the sample is readily identified by the particles contaminating the surface (arrows) in images shown in (A) and (B), (E) and (F).

solvents. These results show that AFM imaging with chemically-modified probes in a controlled environment can produce rationally-interpretable image contrast.

Guntherodt and co-workers pioneered use of friction forces to map different domains in phase-segregated LB films.[37] The image contrast in these investigations, however, arose due to the differences in the elastic properties of the LB film domains and not the chemical functionality at the film surface. It is important to point out that researchers need to use caution when interpreting AFM images as pure maps of surface composition, even when the image is taken with a chemically-modified tip; many systems exhibit complex interactions between the tip and the surface. Only when viscoelastic effects (or site-to-site differences due to them) are eliminated, can the chemical components of the tip-surface interaction dominate and consequently determine the image contrast. Conversely, if the interfacial chemistry is the same, or the probe functionality is chosen to minimize the differences in chemical interactions, then the second order effects (e.g., viscoelastic properties, contact stiffness, etc.) could become dominant.[45]

The conditions under which the imaging is performed are important, since dominant interactions depend on the media even for the same tip-surface system as illustrated by lateral force images of a $COOH/CH_3$ pattern acquired in water and air using a CH_3-functionalized tip in Figures 7H, 7K. The friction contrast between COOH and CH_3 functional groups is relatively large in both images. In water, this pattern shows high friction on the methyl-terminated regions and low friction over the carboxyl-terminated regions of the sample. This result is readily understood on the basis of the friction force measurement that we have discussed in the previous sections. The

contrast reflects the dominant effect of hydrophobic forces (leading to large contact areas) that mask other chemical interactions. Thus imaging under water with hydrophobic CH_3-terminated tips is an approach to constructing hydrophobicity maps of sample surfaces and could be used to map hydrophobic domains on membranes of biological surfaces.

Images acquired in air exhibit friction contrast opposite to those obtained in aqueous solution. It is clear that these images do not reflect chemical interactions directly, but rather are due to large capillary forces between the sample and tip over the hydrophilic COOH-terminated areas of the surface that are wet more readily than CH_3 regions.[35] Although chemical modification of the tip does not influence the contrast controlled by capillary forces, a treatment of AFM probes that produces hydrophobic surfaces can reduce capillary forces and enhance the image resolution.[44, 46, 47] Perhaps the most elegant variation of this approach has been demonstrated by Lieber and co-workers in a series of publications using carbon nanotube AFM probes for high-resolution imaging of colloids and biomolecules. Small size, high aspect ratio, and hydrophobic carbon nanotube sidewalls all contributed to reducing the capillary forces, and, as a result, the CNT probes exhibited minimal adhesion in air, providing extremely stable high-resolution imaging of sample surfaces in ambient conditions.[22, 48–50]

4.2 Tapping Mode Imaging and Energy Dissipation Imaging

Despite conceptual simplicity of the chemical contrast in friction force imaging, practical drawbacks of contact mode imaging are well-known—it exerts unnecessarily high forces on the delicate surfaces of organic or biological samples, thus degrading the imaging resolution significantly, or worse, leading to the tip-induced sample damage. It is not surprising then that AFM has been widely adopted for imaging of such "soft" samples in the intermittent-contact, or "tapping", mode of imaging. In this mode, the AFM probe vibrates near its resonance frequency with substantial amplitude and strikes or "taps" the surface for a brief portion of each oscillation cycle. The resulting images typically exhibit much crisper contrast and the imaging process causes much less surface damage than contact mode imaging. Tapping mode imaging had been broadly adopted for imaging of organic matter, and the origins of the impressive image contrast of the phase component of the tapping mode images were soon established by J. Cleveland and co-workers.[51, 52] They reported the key observation that the phase image contrast reflected the energy dissipation in the tip-sample junction. Specifically, the power dissipated in the tip-sample junction, P_t, is related to the observed phase lag ϕ and cantilever parameters by a simple expression:

$$P_t = \frac{1}{2}\frac{k\omega_0}{Q_{cant}}\left(A_0 A\sin\varphi - A^2\right) \tag{4}$$

or for constant amplitude imaging:

$$\Delta P_t \propto \frac{k\omega_0}{Q_{cant}}\Delta(\sin\varphi) \tag{5}$$

where k is the cantilever spring constant, Q_{cant} is the quality factor, ω_0 is the resonant frequency, and A_0 and A are the cantilever oscillation amplitudes far away from the surface (free vibration) and during imaging (intermittent contact), respectively.

AFM experiments typically feature quite fast loading rates; therefore the tip pull-off from the surface is almost never an equilibrium process. From the point of view of the cantilever dynamics, adhesion interactions measured with soft cantilevers are dissipative,

because the elastic energy stored in the cantilever is dissipated by the viscous damping in the interaction medium after adhesion contact is broken. Therefore, samples presenting areas of large differences in adhesion forces ($\Delta F \propto \Delta P_t$) should produce stronger phase contrast ($\Delta \sin\varphi \approx \Delta\varphi$).

The ability to probe the energy dissipated due to the tip-sample interactions in a direct measurement opened up an opportunity for chemical force microscopy to use tapping mode for probing specific interactions of the functional groups on the AFM probe and the surface of a sample. With the experimental conditions adjusted to minimize the contributions of other interactions (e.g., viscoelastic energy dissipation), the energy dissipated at the probe-surface interface should directly reflect interactions of the chemical functionalities. The first demonstration by Noy et al.[53] of the coupling between adhesion and phase lag in tapping mode images used a familiar model system of interacting self-assembled monolayers on gold surfaces. To keep the variations in the experimental conditions to the minimum, they adjusted the strength of the interactions by varying the composition of the water/methanol medium filling the AFM fluid cell.

Image contrast between sample regions of different composition observed in these measurements was clearly increasing with the increase in the water content (Figure 8). This trend can easily be rationalized by noting that increase in the water content accentuates the differences in the interaction strength between the CH_3-functionalized probe and hydrophobic regions versus hydrophilic regions of the sample.[54] Indeed, a detailed comparison of the observed phase lag with the measured tip-surface interfacial free energies in different solvent mixtures showed a clear correlation between the two (Figure 9). Similarly, Wong et al. observed chemical sensitivity of phase images of COOH/CH_3 SAM patterns obtained using nanotube tips—image contrast inverted when COOH groups at the open ends of CNT were converted to benzyl functionality.[22]

Ashby and Lieber have later refined this approach and developed the Energy Dissipation Chemical Force Microscopy (ED-CFM) approach, where they used an equation similar to Equation 4 construct direct maps of the tip-sample energy dissipation and correlate them to the chemical composition of the tip and surface functional groups.[55] Remarkably, they observed that this approach not only distinguished between the different functionalities on the sample surface, but also aided in removing topography-generated artifacts. A comparison of the amplitude, phase lag, and energy dissipation images of the same region of the sample surface that contains variation in the chemical group functionality and topographic roughness highlights the fact that ED-CFM imaging is considerably more successful in rejecting topographic artifacts than the conventional phase imaging (Figure 10).

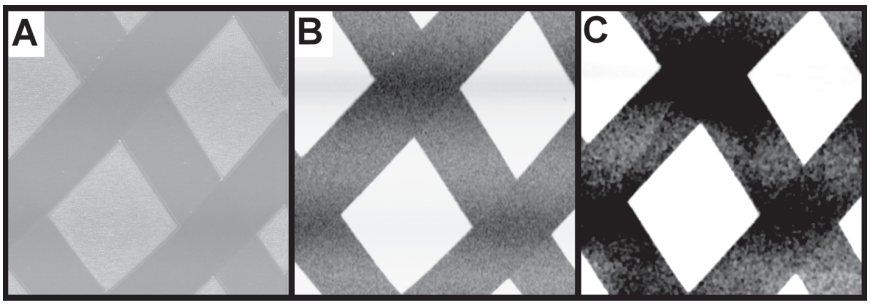

Figure 8. Phase lag maps of a SAM sample patterned with COOH-terminated square regions surrounded by a CH_3-terminated background recorded with the same CH_3-terminated tip in a series of methanol-water solvents. The water content, phase contrast and differences in tip-sample work of adhesion are (A) 20%, (B) 60%, and (C) 80%. The gray scale in each of these 25 μm × 25 μm images represents phase variation of 50°. The imaging set point (A/A_0 ratio) was maintained at 0.6 in all three images.

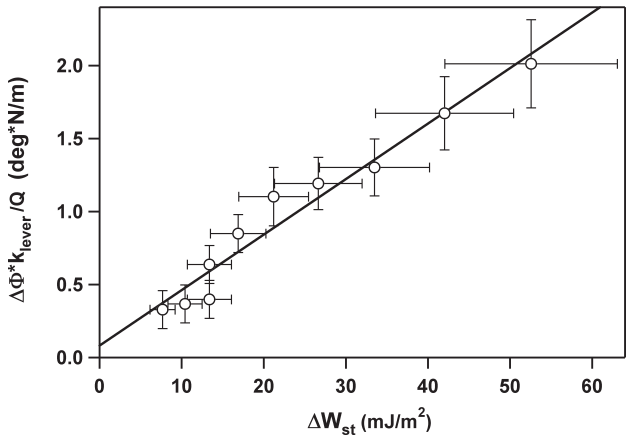

Figure 9. Plot of the product of the cantilever spring constant and phase contrast divided by the cantilever quality factor versus the difference in tip-sample interaction free energies for the two distinct sample regions shown in Figure 8. The data were obtained with an increasing percentage of water from 0 to 80%. The straight line is a linear fit to the data. The plot combines data obtained with two cantilevers having different spring constants and quality factors. Both cantilevers had tips terminating in CH_3 groups. Error bars represent standard deviations determined by bearing analysis of phase lag images and errors in the work of adhesion values originating from uncertainties in the tip radii.

L. Chen et al. have performed further experimental and computational investigations of the AFM probe interactions with the surface in tapping mode imaging and highlighted the importance of controlling the cantilever damping in achieving the highest image resolution.[56] Incorporation of the active methods of controlling such damping (i.e., "Q-control" functionality) directly into the commercial force microscopy instrumentation have already resulted in a further refinement of imaging techniques. It will be interesting to see if it can produce an enhanced ability to separate and isolate the contributions of chemical interactions in chemical force microscopy imaging. Another intriguing possibility arising from the efforts to improve imaging resolution is the use of higher harmonic imaging (i.e., Dual-AC™ mode imaging) that could potentially help to obtain well-defined *quantitative* images of the strength of the tip-sample interactions.

5 Conclusions

Chemically-modified tips produced by covalently linking molecules to force microscope probes proved to be an excellent tool to explore, quantify, and map adhesion and friction forces between complex assemblies of functional groups on a tip and sample. This methodology could also be used to determine the local pK's of surface ionizable functional groups using force titrations with probes bearing groups that undergo dissociation. The interactions observed between modified tip and sample surfaces in aqueous solutions agree well with the predictions of double layer and contact mechanics models. These models can be used to extract surface free energies and double layer parameters that are essential to understanding interactions in aqueous media.

The friction forces between modified tips and samples are also chemically specific; moreover, the magnitudes of the friction forces parallel the trends found for adhesion forces.

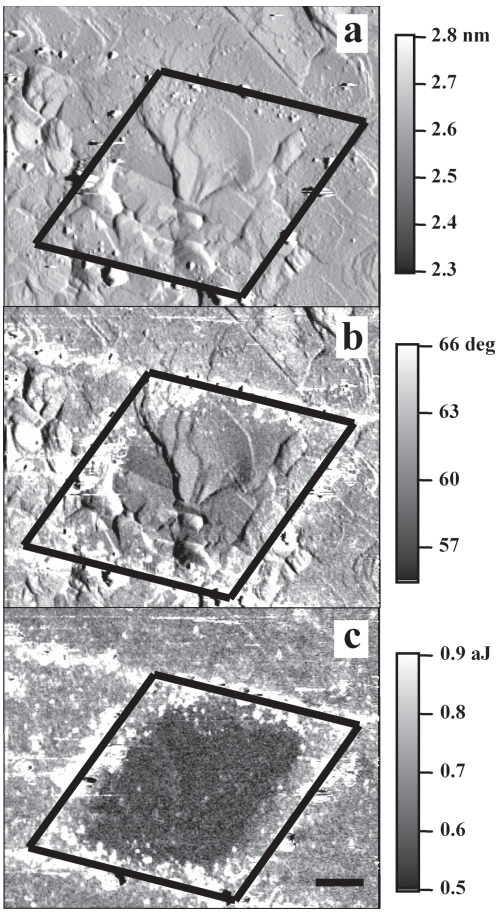

Figure 10. (A) Amplitude, (B) phase lag, and (C) energy dissipation images of a patterned SAM surface of hydroxyl surrounding a carboxyl square. The black square highlights the edges of the pattern. The tip is functionalized with hydroxyl terminated SAM. The images are obtained in 0.01MpH2 phosphate buffer. The topography is coupled into the amplitude and phase images, but compensated in the energy dissipation image. The scale bar at the lower right is 200 nm 55.

This observation underscores the fundamental role of the basic non-covalent interactions in shaping microscopic mechanisms of surface phenomena such as adhesion and friction. The parallels between the two phenomena extend also to force titrations: friction between ionizable groups changes upon dissociation of interacting functionalities; for example, the friction forces for COOH-terminated surfaces decreased significantly at a pH corresponding to the pK_a determined from the adhesion measurements.

Significantly, this predictable dependence of friction forces on the tip and sample functionality could form the basis for chemical force microscopy where lateral force images are interpreted in terms of the strength of adhesive and shear interactions between functional groups. Therefore, in conjunction with adhesion data, CFM can distinguish different functional group domains in organic and aqueous solvents. When present, the hydrophobic effect dominates both adhesion and friction forces, and hence lateral force images taken with methyl-terminated tips in aqueous solutions can map hydrophobic regions on a sample. On hydrophilic surfaces, observed pH-dependent changes in friction forces of ionizable groups

can be exploited to map spatial distribution of hydrophilic functional groups and to define their ionization state as a function of pH.

CFM imaging can find many uses in basic and applied research: from quantifying the strength of interactions in host-guest systems to identifying surface distribution of chemical modifications or chemically distinct domains in soft materials such co-polymers. A wide range of intermolecular interactions can be studied by the CFM technique, and analysis of these data can provide basic thermodynamic information relevant to chemical, biological, polymer, and colloidal systems. CFM imaging of systems such as polymers, biomolecules, and other materials could produce direct images of the spatial distribution of functional groups, hydrophobic versus hydrophilic domains, and the time course of the surface reorganization.[57] The approach of using force titrations to determine the local pK of acidic and basic groups may be applicable to probing the local electrostatic properties of protein surfaces in their native environments and the ionization of colloidal particles at the nanoscale. Assignment by CFT of the chemical functionality at the terminus of the shortened carbon nanotube to carboxylic acid groups proves the potential for unparalleled spatial resolution for such identification. Studies using chemically-modified tips also provide new approaches to imaging energy dissipation processes during dynamic (intermittent or sliding) tip-surface contact and will lead to new insights into the molecular mechanisms of dissipative processes relevant to tribology.

6 References

1. *Surface and Colloid Chemistry*; Birdi, K. S., Ed.; CRC Press: Boca Raton, 1997.
2. Myers, D. *Surfaces, Interfaces, and Colloids*; John Wiley & Sons: New York, 1999.
3. Zhmud, B. V.; Golub, A. A. *J. Colloid Interface Sci*. **1994**, *167*, 186.
4. Holmes-Farley, S. R.; Reamey, R. H.; McCarthy, T. J.; Deutch, J.; Whitesides, G. M. *Langmuir* **1988**, *4*, 921.
5. Vezenov, D. V.; Noy, A.; Rosznyai, L. F.; Lieber, C. M. *J. Am.Chem. Soc*. **1997**, *119*, 2006–2015.
6. *CRC Handbook of Chemistry and Physics*; 72 ed.; Lide, D. R., Ed.; CRC Press: Boca Raton, FL, 1991.
7. van der Vegte, E.; Hadziioannou, G. *J. Phys. Chem. B* **1997**, *101*, 9563–9569.
8. Creager, S. E.; Clark, J. *Langmuir* **1994**, *10*, 3675.
9. Chatelier, R.; Drummond, C.; Chan, D.; Vasic, Z.; Gengenbach, T.; Griesser, H. *Langmuir* **1995**, *11*, 4122.
10. Smart, J. L.; McCammon, J. A. *J. Am Chem. Soc*. **1996**, *118*, 2283–2284.
11. Glinski, G. C.; Platten, J. K.; De Saedeleer, C. *J. Colloid Interface Sci*. **1993**, *162*, 129.
12. Zhang, H.; He, H. X.; Wang, J.; Mu, T.; Liu, Z. F. *Applied Physics A:* **1998**, *A66*, S269–S271.
13. Wallwork, M. L.; Smith, D. A.; Zhang, J.; Kirkham, J.; Robinson, C. Langmuir 2001, 17, 1126–1131.
14. He, H.-X.; Huang, W.; Zhang, H.; Li, Q. G.; Li, S. F. Y.; Liu, Z. F. *Langmuir* **2000**, *16*, 517–521.
15. Schoenherr, H.; van Os, M. T.; Foerch, R.; Timmons, R. B.; Knoll, W.; Vancso, G. J. *Chemistr. Mater*. **2000**, *12*, 3689–3694.
16. Schonherr, H.; van Os, M. T.; Vancso, G. J.; Forch, R.; Knoll, W.; Hruska, Z.; Kurdi, J.; Arefi-Khonsari, F. *Chem. Comm*. **2000**, 1303–1304.
17. Zhang, H.; He, H.-X.; Mu, T.; Liu, Z.-F. *Thin Solid Films* **1998**, *327–329*, 778–780.
18. Zhang, H.; Zhang, H.-L.; He, H.-X.; Zhu, T.; Liu, Z.-F. *Mater. Sci. & Engin., C*. **1999**, *C8–C9*, 191–194.
19. Wang, J.; Zhang, H.; He, H.; Hou, T.; Liu, Z.; Xu, X. *Theochem* **1998**, *451*, 295–303.
20. Lee, T. R.; Carey, R. I.; Biebuyck, H. A.; Whitesides, G. M. *Langmuir* **1994**, *10*, 741.
21. Wong, S. S.; Joselevich, E.; Woolley, A. T.; Cheung, C. L.; Lieber, C. M. *Nature* **1998**, *394*, 52–55.
22. Wong, S. S.; Woolley, A. T.; Joselevich, E.; Cheung, C. L.; Lieber, C. M. *J. Am. Chem. Soc*. **1998**, *120*, 8557–8558.
23. Smith, D. A.; Wallwork, M. L.; Zhang, J.; Kirkham, J.; Robinson, C.; Marsh, A.; Wong, M. *J. Phys. Chem. B* **2000**, *104*, 8862–8870.
24. Smith, D. A.; Robinson, C.; Kirkham, J.; Zhang, J.; Wallwork, M. L. *Rev. Analyt. Chem*. **2001**, *20*, 1–27.
25. Smith, D. A.; Connell, S. D.; Robinson, C.; Kirkham, J. *Anal. Chim. Acta* **2003**, *479*, 39–57.
26. Zhang, J.; Kirkham, J.; Robinson, C.; Wallwork, M. L.; Smith, D. A.; Marsh, A.; Wong, M. *Analyt. Chemi*. **2000**, *72*, 1973–1978.
27. Kreller, D. I.; Gibson, G.; vanLoon, G. W.; Horton, J. H. *J. Colloid Interf. Sci*. **2002**, *254*, 205–213.
28. Ashby, P. D.; Chen, L. W.; Lieber, C. M. *J. Am. Chem. Soc*. **2000**, *122*, 9467–9472.
29. Ito, T.; Citterio, D.; Buehlmann, P.; Umezawa, Y. *Langmuir* **1999**, *15*, 2788–2793.
30. Dicke, C.; Hahner, G. *J. Am. Chem. Soc*. **2002**, *124*, 12619–25.

31. Glinski, J.; Chavepeyer, G.; Platten, J. K.; De Saedeleer, C. *J. Colloid Interface Sci*. **1993**, *158*, 382.
32. Chavepeyer, G.; De Saedeleer, C.; Platten, J. *J. Colloid Interface Sci*. **1994**, *167*, 464.
33. Reiner, E. S.; Radke, C. J. *Adv. Colloid Interface Sci*. **1993**, *58*, 87.
34. Overney, R. M.; Takano, H.; Fujihira, M.; Paulus, W.; Ringsdorf, H. *Phys. Rev. Lett*. **1994**, *72*, 3546–9.
35. Noy, A.; Frisbie, C. D.; Rozsnyai, L. F.; Wrighton, M. S.; Lieber, C. M. *J. Am. Chem. Soc*. **1995**, *117*, 7943–7951.
36. Green, J.-B. D.; McDermott, M. T.; Porter, M. D.; Siperko, L. M. *J. Phys. Chem*. **1995**, *99*, 10960.
37. Overney, R. M.; Meyer, E.; Frommer, J.; Brodbeck, D.; Luethi, R.; Howald, L.; Giintherodt, H. J.; Fujihira, M.; Takano, H.; Gotoh, Y. *Nature* **1992**, *359*, 133–135.
38. Berger, C. E. H.; van der Werf, K. O.; Kooyman, R. P. H.; de Grooth, B. G.; Greve, J. *Langmuir* **1995**, *11*, 4188.
39. Xiao, X.; Hu, J.; Charych, D. H.; Salmeron, M. *Langmuir* **1996**, *12*, 235.
40. Lee, G. U.; Chrisey, L. A.; Ferrall, C. E.; Pilloff, D. E.; Turner, N. H.; Colton, R. J. *Israel J. Chem*. **1996**, *36*, 81.
41. Frisbie, C. D.; Rozsnyai, L. F.; Noy, A.; Wrighton, M. S.; Lieber, C. M. *Science* **1994**, *265*, 2071.
42. Wollman, E. W.; Kang, D.; Frisbie, C. D.; Lorkovic, I. M.; Wrighton, M. S. *J. Am. Chem. Soc*. **1994**, *116*, 4395–4404.
43. Wilbur, J. L.; Biebuyck, H. A.; MacDonald, J. C.; Whitesides, G. M. *Langmuir* **1995**, *11*, 825–831.
44. Sinniah, S. K.; Steel, A. B.; Miller, C. J.; Reutt-Robey, J. E. *J. Am. Chem. Soc*. **1996**, *118*, 8925–8931.
45. Dufrene, Y. F.; Barger, W. R.; Green, J. B. D.; Lee, G. U. *Langmuir* **1997**, *13*, 4779–4784.
46. Alley, R. L.; Komvopoulos, K.; Howe, R. T. *J. Appl. Phys*. **1994**, *76*, 5731–7.
47. Knapp, H. F.; Wiegrabe, W.; Heim, M.; Eschrich, R.; Guckenberger, R. *Biophys. J*. **1995**, *69*, 708–15.
48. Wong, S. S.; Woolley, A. T.; Odom, T. W.; Huang, J. L.; Kim, P.; Vezenov, D. V.; Lieber, C. M. *Appl. Phys. Lett*. **1998**, *73*, 3465–3467.
49. Wong, S. S.; Joselevich, E.; Woolley, A. T.; Cheung, C. L.; Lieber, C. M. *Nature* **1998**, *394*, 52–55.
50. Wong, S. S.; Harper, J. D.; Lansbury, P. T.; Lieber, C. M. *J. Am. Chem. Soc*. **1998**, *120*, 603–604.
51. Cleveland, J.; Anczykowski, B.; Schmidt, A.; Elings, V. *Appl. Phys. Lett*. **1997**, *72*, 2613–2615.
52. Anczykowski, B.; Gotsmann, B.; Fuchs, H.; Cleveland, J. P.; Elings, V. B. *Appl. Surf. Sci* **1999**, *140*, 376.
53. Noy, A.; Sanders, C. H.; Vezenov, D. V.; Wong, S. S.; Lieber, C. M. *Langmuir* **1998**, *14*, 1508–1511.
54. Vezenov, D. V.; Zhuk, A. V.; Whitesides, G. M.; Lieber, C. M. *J. Am. Chem. Soc*. **2002**, *124*, 10578–10588.
55. Ashby, P. D.; Lieber, C. M. *J. Am. Chem. Soc*. **2005**, *127*, 6814–6818.
56. Chen, L.; Cheung, C. L.; Ashby, P. D.; Lieber, C. M. *Nano Lett* **2004**, *4*, 1725–1731.
57. Hillborg, H.; Tomczak, N.; Olah, A.; Schonherr, H.; Vancso, G. J. *Langmuir* **2004**, *20*, 785–794.